ELSEVIER

Modelling unsaturated flow in an evolving karst aquifer

Georg Kaufmann

Institut für Geophysik, Universität Göttingen, Herzberger Landstrasse 180, 37075 Göttingen, Germany

Abstract

A two-dimensional cross-section of a karst aquifer, in which chemical dissolution enlarges fractures with time, is studied. The karst aquifer is recharged by precipitation and drains towards a resurgence. The initial aquifer has low conductivities both in the rock matrix and the fracture network, and the initial water table is high. As the enlargement of fractures by dissolution increases the fracture conductivity, the water table drops, until it reaches a steady-state along the level of the resurgence. Several parameterisations are discussed for flow in the unsaturated zone above the water table. It is shown that different approaches result in similar cave passage patterns, with a large water-table cave draining the recharge towards the resurgence. However, flow patterns in the unsaturated zone can be very different for the different parameterisations.
© 2003 Elsevier Science B.V. All rights reserved.

Keywords: Karst aquifer; Limestone dissolution; Cave genesis; Hydraulic conductivity

1. Introduction

The evolution of a karst aquifer is characterised by a change in the flow regime. During the early phase of evolution, flow both in the rock matrix and in small fissures is comparable, and the aquifer responds as a homogeneous, pore-controlled medium. After fissures are chemically enlarged by calcite dissolution, flow is channelled through the fissure system and the aquifer becomes a heterogeneous, fracture-controlled medium.

Several processes control the evolution of the karst aquifer: (i) The rate of fracture enlargement in the limestone is controlled by the dissolution chemistry in the ternary system calcite–carbon dioxide–water. Water enriched in carbon dioxide dissolves calcite

within the limestone aquifer. The rate of dissolution depends on the water chemistry and is controlled by temperature, carbon dioxide pressure, calcium concentration, and fissure width. (ii) The tectonic setting guides the enlargement in the aquifer, as the initial width of fractures and the density of fracturing are important parameters for the evolution of subsurface flow. (iii) Groundwater recharge and discharge drives the flow through the aquifer, as the amount of recharge, either by precipitation or sinking streams, and the height of the base level of resurgences and rivers, establish the pressure difference for flow within the aquifer.

A karst aquifer is difficult to access, especially in its early evolution. Only sufficiently enlarged fractures can be explored by humans, and provide a limited knowledge of the fracture distribution in a catchment area. As fracture width in the early

evolution is within the millimetre to centimetre-range, no direct observations are possible. Here, numerical modelling of the evolution of a karst aquifer provides an important tool to study the enlargement of fractures and the evolution of flow in the karst aquifer. Over the past decade, several numerical models have been discussed in the literature.

In a first generation of one-dimensional models for single fracture enlargement (e.g. Dreybrodt, 1990; Palmer, 1991; Groves and Howard, 1994a), the importance of high-order kinetics for the dissolutional enlargement has been established. Subsequent modelling then focused on the early evolution of two-dimensional fracture networks of karst aquifers with simple boundary conditions (e.g. Groves and Howard, 1994b; Howard and Groves, 1995; Hanna and Rajaram, 1998; Siemers and Dreybrodt, 1998). In this generation of models, the recharge condition proved to be another important parameter for the evolution, with fixed head boundary conditions simulating a hydraulic control resulting in more rapid and complex passage patterns than fixed recharge boundary conditions simulating a catchment control situation. Emphasis then shifted to more complex models simulating flow in fractured, porous networks and more realistic recharge boundary conditions (e.g. Clemens et al., 1996, 1997; Kaufmann and Braun, 1999, 2000; Gabrovsek et al., 2000). These models revealed the importance of the porous matrix flow component in the early phase of karstification, and were able to reproduce models of branch-work caves as proposed by Palmer (1991) under catchment flow conditions. Finsterle (2000) has compared responses of a discrete fracture model and a continuum model with heterogeneous permeability and concluded that in aquifers with strongly preferential flow paths (such as karst aquifers)the continuum model is inappropriate. Hence there is a need to model the fracture distribution explicitly in an evolving karst aquifer.

The above two-dimensional models all depend on the imposed tectonic setting, which guides the evolving fracture network in the aquifer. Also, all models assume that during the aquifer evolution the entire aquifer network remains flooded to maintain phreatic conditions, while in reality the water table will drop with increasing permeability of the fractures.

A first numerical study accounting for a fluctuating water table has been carried out by Gabrovsek and Dreybrodt (2001). In this study, passage enlargement within the karst aquifer is mainly occurring around the water table, and hence the early drop of an initially high water table to a steady-state base level niveau leaves a zone of enlarged vadose fractures, and the possibility of a phreatic passage evolving along the steady-state water table. For a fixed recharge boundary condition, the water table quickly drops to base-level niveau, and a phreatic passage grows from the resurgence headwards. In contrast, for fixed head boundary conditions the water table remains high, and enlargement results in passages steeply dropping towards the resurgence. Accounting for a fracture network with variable initial widths, Gabrovsek and Dreybrodt (2001) concluded that competition between enlargement of more prominent fractures and tight fractures along the water table determines the aquifer evolution. A time-dependent water table has also been modelled by Bauer et al. (2000, 2001) to simulate the genesis of cave systems with an incising base level. However, both Gabrovsek and Dreybrodt (2001) and Bauer et al. (2000, 2001) have neglected flow in the unsaturated zone by inserting the recharge directly along the time-dependent water table. Hence, flow in the entire area above the water table is ignored in these models.

In Kaufmann (2002), a vertical aquifer with time-dependent water table was modelled. The karst aquifer receives a constant recharge along the top boundary by precipitation, and drains towards a resurgence assumed to be the base level in a valley. Flow is allowed both in the permeable rock matrix and the fracture network, and the fractures are enlarged with time by chemical dissolution. Hence, during the early evolution of the karst aquifer the conductivity increases over several orders of magnitude, and the initially high water table drops to a steady-state base-level niveau. As a consequence, fractures above the final water table change from phreatic to vadose flow conditions. While in the models flow through the vadose zone has been taken into account, no dissolution was allowed in the vadose zone. Kaufmann (2002) has carried out a parameter study to investigate the aquifer evolution over a wide range of parameters, such as recharge rate, initial fracture width and density, and initial calcium concentration.

The numerical models cover a wide range of drainage patterns, from phreatic water-table caves, deep bathyphreatic caves, to vadose river caves.

In this paper, we extent the work of Kaufmann (2002) and we propose several scenarios to model the flow pattern in the unsaturated zone of the karst aquifer. Our emphasis is to provide several alternative concepts to model flow in the unsaturated, vadose zone, and compare these concepts in terms of fracture evolution and drainage patterns. The modelling of flow in the unsaturated zone is still poorly understood, and our conceptual models should therefore stimulate further discussion on the model validity.

2. Theory

Flow in a cross-section of a vertical karst aquifer is modelled using the discrete fracture approach (e.g. Gureghian, 1975; Huyakorn et al., 1983), which incorporates fractures directly into the medium. The advantage of the discrete fracture approach is the combined modelling of matrix and fracture elements and the consistent modelling of flow in the matrix-fracture medium.

A transient Poisson equation is used to characterise flow in the fractured, porous karst aquifer:

$$\frac{\partial}{\partial x}\left(bK\frac{\partial h}{\partial x}\right) + \frac{\partial}{\partial z}\left(bK\frac{\partial h}{\partial z}\right) = S\frac{\partial h}{\partial t} - q. \tag{1}$$

Here, x and z are the horizontal and vertical coordinate directions, t is time, h is the hydraulic head in the model domain, K, b, and S are the conductivity, the aquifer thickness and the storage coefficient of the aquifer, and q is the recharge. The product bK controls the flow, hence for simplicity we choose a nominal aquifer thickness of $b = 1$ m. The recharge is derived as the fraction of precipitation, which contributes to the replenishment of the water table. For an average mid-latitude climate, around 50% of the precipitation is available for recharge; the rest is evapotranspiration. For a total of N nodes in the model domain, (1) represents a set of N equations for the N unknown heads h_i at nodes i.

In the vertical aquifer scenario, the hydraulic head h_i comprises the pressure head p_i and the elevation head z_i

$$h_i = p_i + z_i. \tag{2}$$

The elevation head is the altitude of the node i. Hence, we distinguish between the saturated (phreatic) zone for $h_i \geq z_i$, and the unsaturated (vadose) zone for $h_i < z_i$. The condition $h_i = z_i$ defines the water table ($p_i = 0$). We make use of the water-table definition $p_i = 0$ to account for the reduced conductivities in the unsaturated zone:

$$K = \begin{cases} K_s, & h_i \geq z_i, \quad p_i \geq 0, \\ K_r K_s, & h_i < z_i, \quad p_i < 0, \end{cases} \tag{3}$$

with K_s the conductivity in the saturated zone, and K_r the relative conductivity in the unsaturated zone. Several competing relations for the relative conductivity can be found in the literature (e.g. Mualem, 1976; Brooks and Corey, 1964):

$$K_r = \begin{cases} \Theta_e^{0.5}[1 - (1 - \Theta_e^{1/m})^m]^2 & \text{M,} \\ \Theta_e^{3+(2/\lambda)} & \text{BC.} \end{cases} \tag{4}$$

Here, the effective water content Θ_e is defined as (e.g. van Genuchten, 1980)

$$\Theta_e = \Theta_r + (\Theta_s - \Theta_r)\Theta, \tag{5}$$

with Θ_s the saturated water content, Θ_r the residual water content, and Θ the water content function, which can be parameterised as follows (e.g. Gardner and Mayhugh, 1958; Brooks and Corey, 1964; van Genuchten, 1980; Istok, 1989):

$$\Theta = \begin{cases} e^{\alpha p}, & \text{A,} \\ \left[\dfrac{1}{1 + (\alpha + |p|)^n}\right]^m & \text{B,} \\ (1 + \alpha|p|)^{-\lambda} & \text{C.} \end{cases} \tag{6}$$

Here, α is a constant derived from field observations, and the exponents m, n and λ are related through (van Genuchten, 1980)

$$m = 1 - \frac{1}{n}, \qquad \lambda = nm. \tag{7}$$

From Eq. (6) we find that the reduction of conductivity in the unsaturated zone depends on the distance to the actual water table. For parameters as defined in Table 1, the effective water content for all three parameterisations given in Eq. (6) rapidly declines for negative pressure heads (Fig. 1). While relations B and C result

Table 1
Reference model parameters

Parameter	Description	Unit	Value
q	Recharge rate	mm yr^{-1}	1000
K^m	Matrix conductivity	m s^{-1}	1×10^{-7}
S^m	Matrix storage	–	0
S^c	Fracture storage	–	0
b	Aquifer thickness	m	1
c	Initial calcium concentration	mol cm^{-3}	$0.9 \times c_{eq}$
d_{ini}	Initial fracture diameter	mm	0.15
g	Gravitational acceleration	m s^{-2}	9.81
ν	Kinematic viscosity	$\text{m}^2\,\text{s}^{-1}$	1.14×10^{-6}
α	Unsaturation constant	m^{-1}	0.01
n	Power-law exponent	–	2
θ_r	Residual water content	–	0
θ_s	Saturated water content	–	1

in relatively similar reductions, relation A drops faster. As a result, the relative conductivity for relation A (with $m = 1$) drops by three to four orders of magnitude for pressure heads down to $p \simeq -1000$ m, while for relations B and C relative conductivities drop faster for smaller pressure heads and reach a reduction of four to five orders of magnitude for $p \simeq -1000$ m.

The set of equations (1) is solved with a Galerkin finite element method, with triangular three-node elements for the porous rock matrix, and linear two-node elements for the fractures. The triangular matrix elements consist of nodes i, j, m given in the global coordinate system (Fig. 2), and the properties are given as conductivity K^m and storativity S^m. The linear

fracture elements connecting i and j are derived in the local fracture coordinate system, their properties are given as conductivity K^c and a storativity of $S^c = 0$. As the timescale considered for the karst aquifer evolution is long (a few thousand years) when compared to the timescale of storage capacity, flow in the porous rock matrix can also be treated as quasi-static, thus $S^m = 0$. We numerically model dissolution and flow at one year time steps, as a further reduction in the flow time step does not change the calculation.

The conductivity of the fractures is time-dependent, $K_s^c = K_s^c(t)$, as the fractures are enlarged by chemical dissolution. We treat the fractures as circular conduits, thus

$$K_s^c(t) = \frac{g}{32\nu}[d(t)]^2. \tag{8}$$

Here g is the gravitational acceleration, and ν the kinematic viscosity of the solution. The diameter of the fracture $d(t)$, is time-dependent, and the enlargement depends on the calcium dissolution rate in the fracture. In the ternary system calcite–water–carbon dioxide, $CaCO_3$–H_2O–CO_2, the calcium dissolution rate is controlled by various rate-limiting processes, such as the slow hydration of CO_2 into carbonic acid, the dissolution of calcium, Ca^{2+}, at the solution–rock interface, and mass transport through diffusion of the dissolved species within the solution. Depending on the thickness of the water film on the rock surface and the calcium concentration, $[Ca^{2+}]$, in the solution, the calcium fluxrate is given as
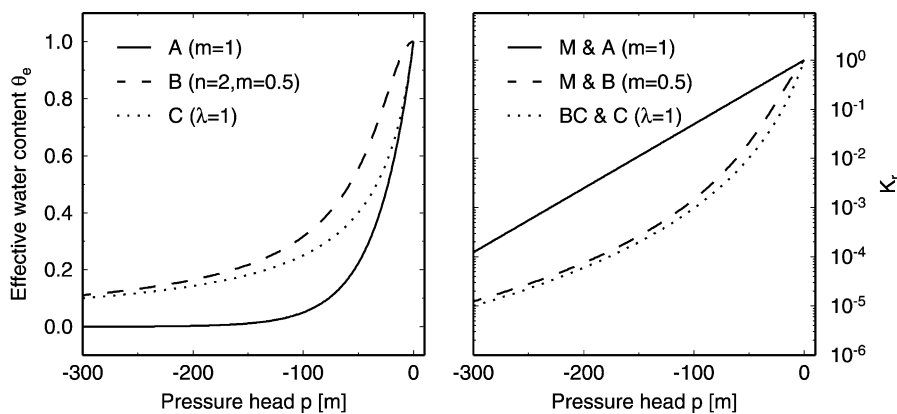

Fig. 1. Effective water content Θ_e and relative conductivity K_r as a function of pressure head p for three different water-content laws. The saturation length is $\alpha = 0.03$.
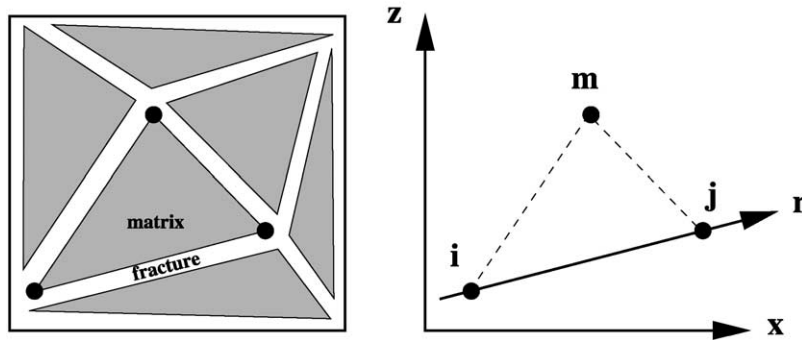
Fig. 2. Conceptual model of fractured, porous aquifer (left) and geometrical realisation (right). Global x–z coordinate system for the porous matrix blocks with nodes i, j, m, and a local r coordinate system for a single fracture between nodes i and j are shown.

$$F_{\mathrm{Ca^{2+}}} = k_i\left(1 - \frac{c}{c_{\mathrm{eq}}}\right)^{n_i}, \quad i = 1, 2, \tag{9}$$

where $c_{\mathrm{eq}} = 2 \times 10^{-6}$ mol cm^{-3} is the equilibrium concentration. For calcium concentrations below a threshold $c_{\mathrm{s}} = 0.9c_{\mathrm{eq}}$, Eq. (9) is modelled as a linear relation (e.g. Dreybrodt, 1996),

$$n_1 = 1, \qquad k_1 = k_0\left(1 + \frac{k_0\delta}{6Dc_{\mathrm{eq}}}\right)^{-1}, \tag{10}$$

with the rate coefficient $k_0 = 4 \times 10^{-11}$ mol cm^{-2} s^{-1}, the diffusivity $D = 10^{-5}$ cm^2 s^{-1}, and δ the thickness of the water film (in cm), which in our model increases with time. For calcium concentrations above the threshold, the calcium flux rate follows a power-law (Palmer, 1991),

$$n_2 \simeq 4, \qquad k_2 = k_1\left(1 - \frac{c_{\mathrm{s}}}{c_{\mathrm{eq}}}\right)^{(n_1 - n_2)}. \tag{11}$$

Note that k_2 is several orders of magnitude larger than k_1, but the high-order flux rate above the threshold remains much smaller than the low-order flux rate valid for smaller calcium concentrations due to the power-law introduced by $n_2 = 4$ in Eq. (9). While we assign an initial calcium concentration at the recharge locations, concentrations at fracture intersections are mixed volumetrically. Then, from the calcium flux rate and the flow rates within the aquifer, we can calculate the evolution of the fracture diameter, $d(t)$. The numerical implementation of the solutional widening of the fracture represented as a circular conduit is described in detail in Kaufmann and Braun

(1999). All typical model parameter values are given in Table 1.

3. Model

The conceptual model resembling a two-dimensional cross-section of a karst aquifer is sketched in Fig. 3. The plateau surface receives a spatially uniform recharge, q. The resurgence located at the base of a valley is defined by a constant head boundary condition, $h_1 = $ const, which is equal to the corresponding topographical height of the resurgence. A seepage face above the resurgence is allowed.
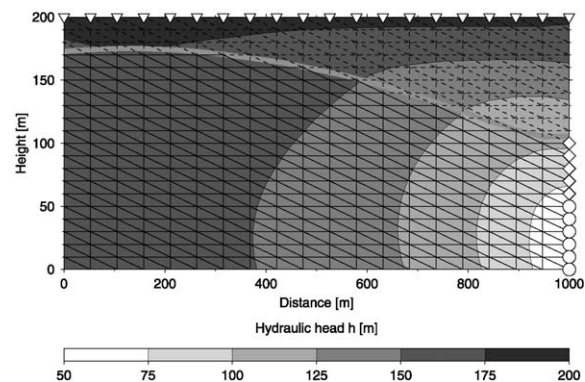

Fig. 3. Conceptual model of the cross-section of the fractured, porous karst aquifer. The plateau surface along the top boundary receives a spatially constant recharge (triangles), the base level is given as a resurgence in the valley (dots), and above the resurgence a seepage face is present (diamonds). Phreatic fractures are shown as black lines, vadose fractures as dashed lines, and the triangles are the porous rock matrix. Hydraulic heads are contoured, and the thick line depicts the initial water table.

The model domain is discretised into a set of N nodal points with coordinates (x_i, z_i), $i = 1, N$. The x-coordinate is the horizontal, the z-coordinate the vertical dimension of the aquifer. The resulting fracture network comprises sets of horizontal bedding partings, vertical fractures, and a set of inclined fractures tilted towards the base level (see Fig. 3).

The cross-sectional model domain has a nominal length of 1000 m, and a total height of 200 m. With 420 nodal points chosen, the fracture spacing is 50 m in horizontal and 20 m in vertical direction. Both the left and the bottom boundary are no-flow boundaries, the top boundary is characterised by a fixed inflow, and the right boundary has a fixed head below the base level, and a seepage face above the resurgence. The resulting distribution of hydraulic heads in the model domain is used to determine the water table, which separates the saturated zone from the unsaturated zone (see Fig. 3). The water table increases from around 100 m on the right side, with a seepage face above the resurgence, to almost 160 m along the left side. In Fig. 3, the head distribution is also shown. Hydraulic heads increase from around 50 m on the resurgence side to almost 200 m in the top left corner. Flow is directed from the recharge points along the top towards the resurgence.

As the fractures enlarge with time, the initially high water table drops and reaches a steady-state water table along the base level. Based on the time-dependent water table in the model domain, the fracture system below the water table is defined as fully flooded with flow driven by pressure differences (phreatic conditions), and the fractures above the water table as conduits with flow driven by gravitation (vadose conditions). As the discretisation of the problem results in fractures crossing the water table, a definition needs to be made for their fate. In this paper, these fractures are treated as already vadose.

4. Results

In this section, we discuss several model runs with different model assumptions. For all models, the physical size of the aquifer, the initial conductivities, fracture distributions, and base level are kept fixed. Differences arise from the way the unsaturated zone is modelled (is it present?, is it evolving?), and

the recharge condition (along the top boundary or along the water table?).

4.1. Run 1: recharge along water table, no vadose zone

With the first run we mimic the models chosen by Gabrovsek and Dreybrodt (2001) and Bauer et al. (2000, 2001) by injecting the recharge always along the actual water table. We argue is this case that the recharge is channelled down through the vadose zone effectively through enlarged vertical fissures and shafts, and all surface recharge replenishes the water table directly. However, we do not use the information on the heterogeneous conductivity of the vadose zone resulting from the model itself. With this approach, we guarantee that flow passes through the vadose zone vertically and recharges the water table, but we ignore vadose passages, which have evolved earlier.

After 1000 years (Fig. 4a), the set of enlarged fractures is present in the unsaturated zone, and the water table has dropped significantly, already reaching the base level along the right part of the aquifer. In this part, a water table cave has started evolving, growing from the resurgence headwards. As recharge is injected along the water table, the maximum flow velocities are present along the water table (Fig. 4b). The main flow is guided through sub-horizontal phreatic fractures along water table, and then fed into enlarged fractures along the base level in the right part of the aquifer, draining towards the resurgence. Note that the apparent upward flow velocities result from water passing through bathyphreatic loops (a dipping conduit draining into a short vertical fracture). No flow occurs above the water table. After 2000 years (Fig. 4c), the water table has dropped further, and the water-table cave has captured flow halfway back into the aquifer. After 50,000 years (Fig. 4e), the water table has reached its steady-state level, and the water-table cave occupies the entire model length. As recharge is injected only along the water table, flow is now entirely guided through the water-table cave (Fig. 4f). In fact, this scenario is now similar to the one-dimensional analogon of a single evolving fracture. This is also evident from the missing flow velocities in the vadose zone, which by know is completely bypassed in this model.
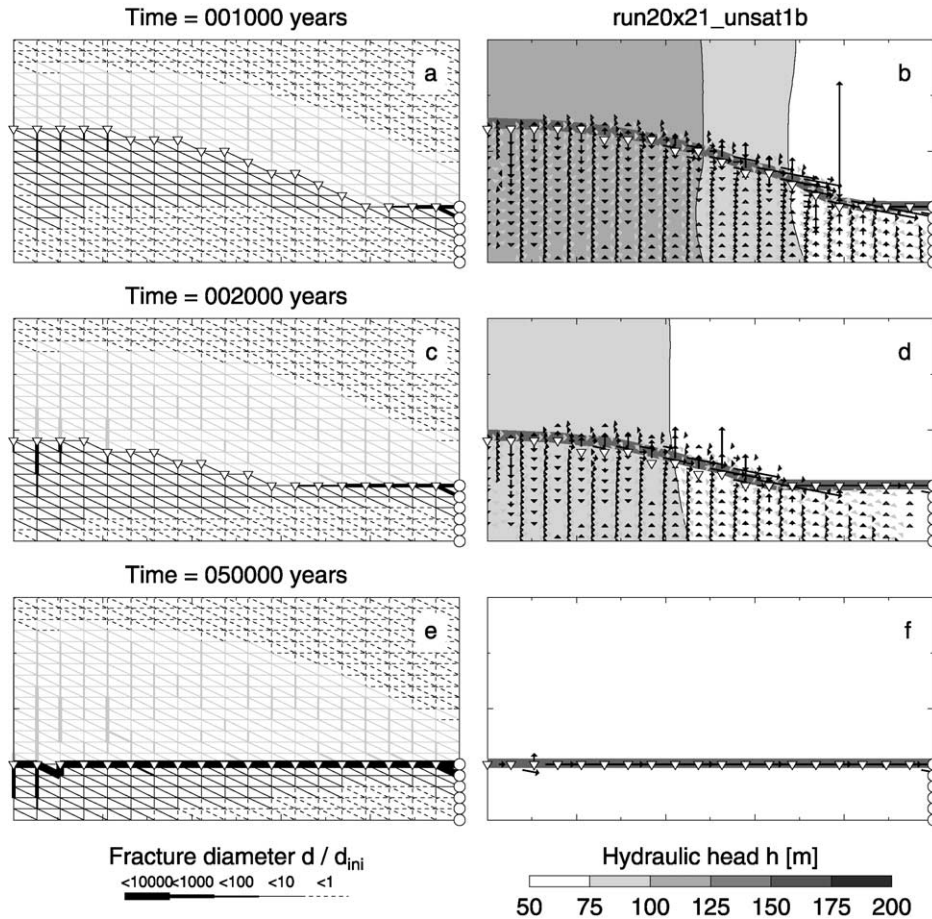
Fig. 4. Run 1: recharge along water table (triangles), no vadose zone, discharge to base level (dots) along right boundary. Thick grey lines indicate the water table, black and grey lines are evolved fractures, with grey lines indicating fractures in the unsaturated (vadose) and black lines fractures in the saturated (phreatic) zone. The line thickness corresponds to the width of the fracture. Black and grey arrows represent flow velocities in the matrix and fractures, respectively.

In Fig. 5a, fracture diameter properties are shown as a function of time. The maximum diameter monitors the evolution of the largest fracture in the aquifer. The maximum diameter increases from its initial value of 0.15 mm to almost 1 m during the 50,000 years of modelling time. In contrast, the average fracture diameter grows slowly during the first 1000 years, as the water table drops fast during that time and inactivates fracture grow in the unsaturated zone. From then on, the average fracture diameter increased sharply, as the water-table cave starts evolving and the same set of fractures remain active from that time onwards. The base-level diameter indicates growth of fractures along the final steady-state water table. During the initial phase of lowering of the water table, this parameter increases slower than the maximum diameter, as enlargement is occurring everywhere below the water table. When the water table has dropped to its steady-state level after 2000 years, enlargement is restricted to the fractures along the steady-state water table. Consequently, the base-level diameter increases rapidly, until it reaches the maximum diameter value. In Fig. 5b, the evolution of the maximum and average heads is shown. Both values decrease with time, as the aquifer becomes more permeable. After the water table has fallen to its
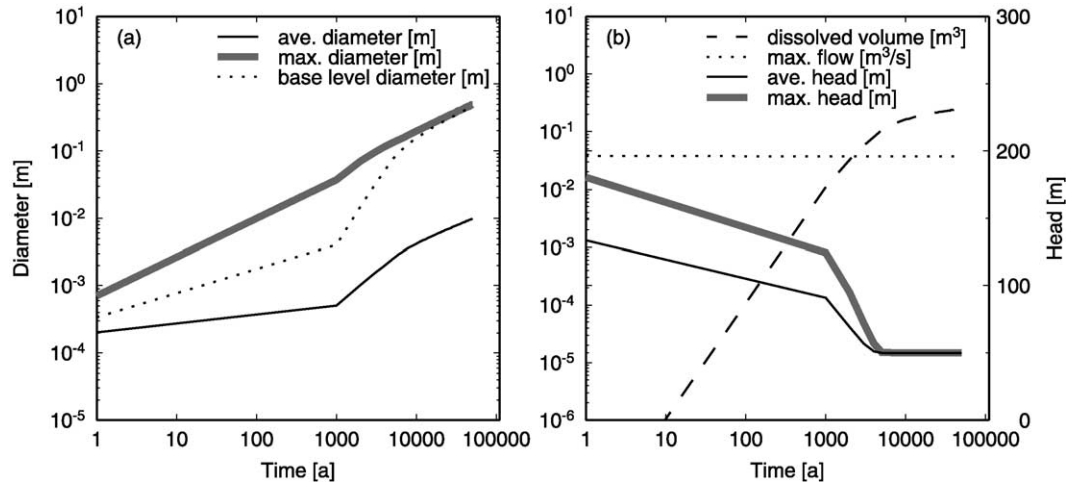
Fig. 5. Run 1: statistical properties.

steady state, both the maximum and the average head drop sharply and reach the base level. During the early state of the evolution, the total dissolved volume increases sharply. The dissolved volume then increases more slowly after the water table has reached its steady-state, as the water-table cave grows at a constant pace.

We now make models more complicated in several steps, as we take flow above the water table into account in the models. Two effects are discussed: The influence of modelling conductivity in the unsaturated zone, and possible dissolution in the vadose fractures. Our aim is to find a model parameterisation, which resembles the gravitationally driven vertical flow in the unsaturated zone, and which does not need to make too strict approximations.

4.2. Run 2: surface recharge, vadose zone (A, $\alpha = 0$) with no enlargement

We need to adopt different strategies for the modelling of flow and dissolution in the unsaturated zone. In the second run, we recharge the system along the top boundary, but we neglect fracture enlargement in the unsaturated zone. Note that the unsaturated zone in this run is characterised solely by the location of the water table, as conductivities in the unsaturated zone remain unchanged at saturated values ($K_r = 1$). In this model, which is similar to the models discussed in Kaufmann (2002), the water is passing through the unsaturated zone without enlarging fractures. However, the region between the initial and the final water table, which was initially phreatic but became vadose at later stages, has been enlarged during the early phreatic stage, and hence influences the flow through the vadose zone. This effect can be seen in Fig. 6a–f. Here, the water table during the first couple of thousand years drops from its initially high position to its steady-state, leaving behind a zone of enlarged fractures. As a consequence, flow in the unsaturated zone is controlled both by matrix flow in areas where no significant enlargement of fractures occurred (e.g. above the water table), and through fractures at locations where the increased fracture diameter provides a more efficient drainage. The unsaturated zone becomes very heterogeneous and a significant amount of flow is guided along horizontal and dipping fractures, resulting in unrealistic deviations from the vertical flow component towards the water table (e.g. Fig. 6d and f). At the end of the model evolution after 50,000 years, the water table has reached the steady-state level, and again a water-table cave has evolved. The difference to run 1, however, is that flow into the water-table cave is guided in parts through dissolutionally enlarged fractures, and hence the water-table cave receives non-uniform recharge.
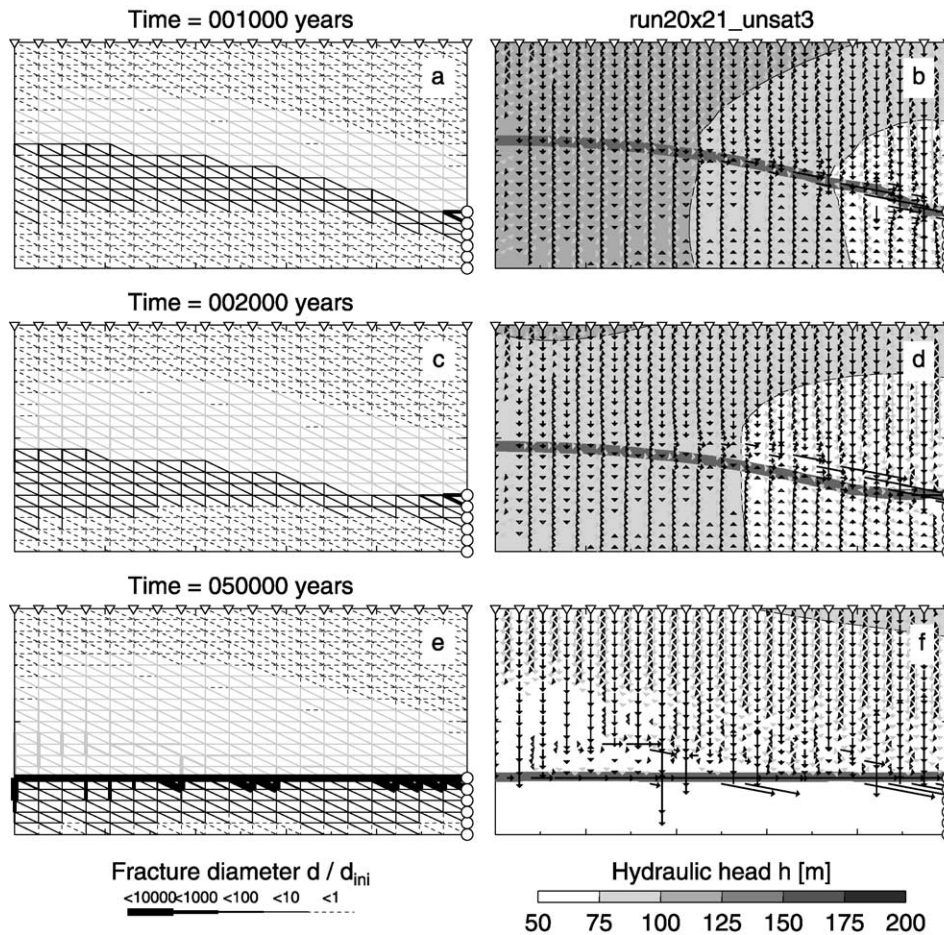
Fig. 6. Run 2: recharge along top boundary (triangles), vadose zone (A, $\alpha = 0$), but no dissolution, discharge to base level (dots) along right boundary.

The statistical properties shown in Fig. 7 show the two-step evolution of the system. During the early phase, when the water table is falling, the maximum diameter is growing, mainly because of enlargement close to the resurgence, but the average diameter evolution is very low, as fractures are slowly enlarged, then become dry due to the falling water table and enlargement moves down to new lower levels. During this early phase, the base-level diameter is almost constant and low. Once the water table has dropped to its steady-state level, the base-level diameter evolution increases sharply, as a water-table cave evolves, growing headwards from the resurgence. Both the maximum and the average heads decline slowly during the early phase of evolution, but they drop sharply, once the water table has dropped to its final steady-state position and the water-table cave starts evolving. However, the maximum head remains higher than the average head during the entire evolution modelled, as due to the recharge along the top boundary it is possible to maintain a pressure difference across the aquifer.

The strong deviation of flow in the unsaturated zone away from the vertical direction is of course not observed in nature. The non-vertical flow in the model is caused by the strong heterogeneities in conductivity in areas, where fractures have been enlarged in the early phreatic phase. Hence, our next aim is to force flow vertically downward,
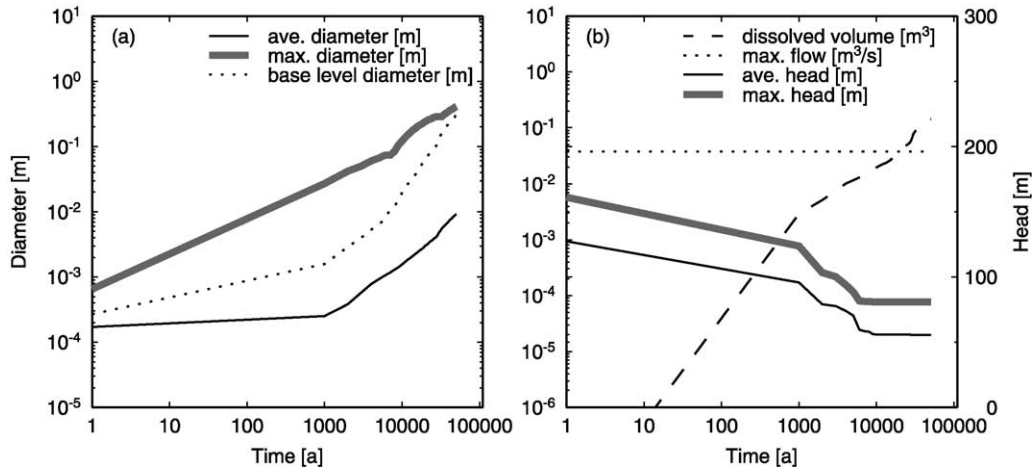
Fig. 7. Run 2: statistical properties.

bypassing the old highly permeable zones above the water table.

4.3. Run 3: surface recharge, vadose zone (A, $\alpha = 0.03$) with no enlargement

We proceed by decreasing the conductivities in the unsaturated zone according to relation A for the water-content function given in Eq. (6) and a relative permeability following relation M in Eq. (4) for $m = 1$. The remaining parameters are chosen as in Table 1. This reduction in conductivity is used to force the recharge on a more vertical path through the vadose zone. The results for this third run are shown in Fig. 8a–f. After 1000 years (Fig. 8a), the water table has dropped, leaving behind a vadose zone with enlarged fractures as in run 2. However, the different modelling of the unsaturated zone results in a different head distribution, as it can be seen in Fig. 8b. Hydraulic heads in the top part of the aquifer are still high, and head isolines are almost horizontal and subparallel to the surface. As a consequence, flow in the top part is directed vertically downward towards the phreatic zone, both in the matrix and the fissures. However, when flow reaches significantly enlarged, now vadose fractures, it is still channelled and diverted away from the vertical direction, following the enlarged fracture directions. After 50,000 years the water table has reached its steady-state level (Fig. 8e),

and a large water-table is evolving, as in the previous scenarios.

In Fig. 9a, the evolution of fracture diameter properties are shown. When comparing the curves to the one from run 2 (Fig. 7a), both the average and the maximum diameter are very similar. Differences occur for the base-level diameter, which grows faster for run 3 in the early phase, until the steady-state water table is reached at 1000 years. From then on the base-level diameter quickly converges towards the maximum diameter value. The faster growth during the early phase is related to higher hydraulic heads in the unsaturated zone. While the dissolved volume and the average head, shown in Fig. 9b, evolve similar to the one for run 2, the maximum head for run 3 remains significantly higher than in run 2. This larger value clearly reflects the high hydraulic heads in the unsaturated zone, which are responsible for the downward flow component.

We have also tested the model with different unsaturation constants ($\alpha = 0.01$ and $\alpha = 0.05$). While the intensity of the vertical flow component changes, the evolution finally converged to the water-table cave as shown in Fig. 8e. While the distribution of fractures resulting from runs 2 and 3 is not very different, the typical downward flow through the top part of the unsaturated zone, with large hydraulic head differences underneath the surface, is a characteristic feature of the modelling approach with unsaturated conductivity. Still, flow deviates from the vertical
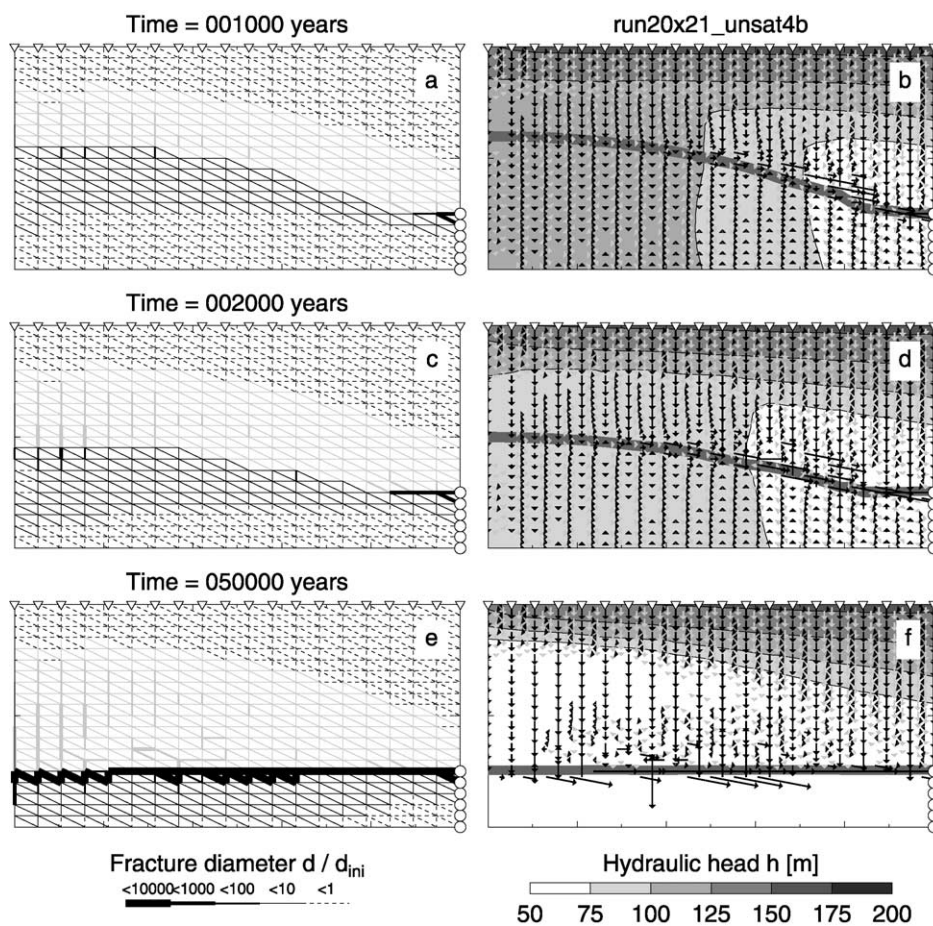
Time = 001000 years   run20x21_unsat4b

Time = 002000 years

Time = 050000 years

Fracture diameter d / d_{ini}

<10000 <1000 <100 <10 <1

Hydraulic head h [m]

50 75 100 125 150 175 200

Fig. 8. Run 3: recharge along top boundary (triangles), vadose zone (A, $\alpha = 0.03$), but no dissolution, discharge to base level (dots) along right boundary.
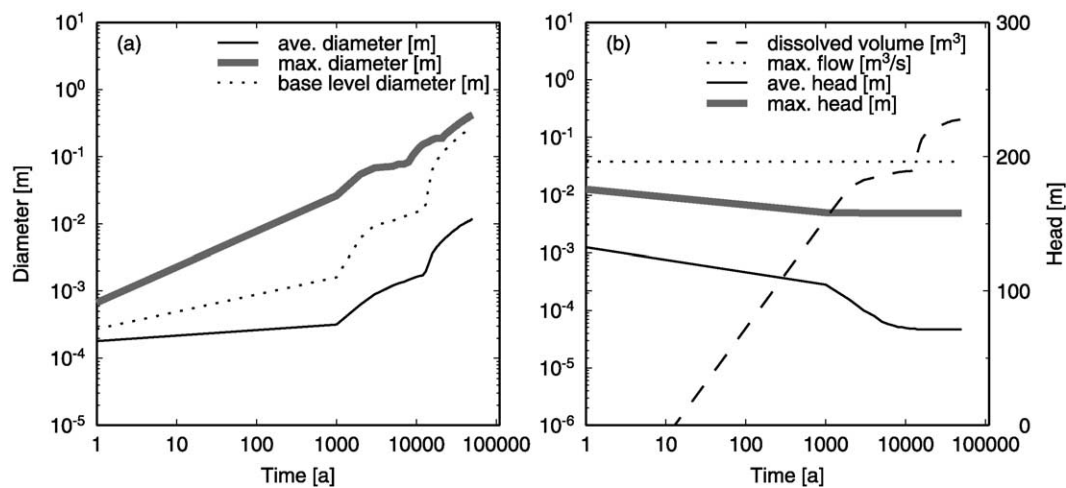

(a)   ave. diameter [m]
      max. diameter [m]
      base level diameter [m]

(b)   dissolved volume [m³]
      max. flow [m³/s]
      ave. head [m]
      max. head [m]

Fig. 9. Run 3: statistical properties.

directions closer to the water table, which is unrealistic and needs to be addressed better.

4.4. Run 4: surface recharge, vadose zone (B, $\alpha = 0.03$) with no enlargement

With the fourth run, we test a different parameterisation for modelling the unsaturated zone, using relation B for the water-content function given in Eq. (6) and a relative permeability following relation M in (4) with n given in Table 1. As we have seen in Fig. 1, relation B reduces the conductivity faster than the exponential relation A, hence the unsaturated zone is less permeable than in run 3. The results for this fourth run are shown in Fig. 10a–f. While the fracture evolution results in similar fracture distributions as in the previous run 3, with a water-table cave

evolving after the water table has dropped to its steady-state position, the vertical flow component in the unsaturated zone has intensified, when compared to run 3. Also, hydraulic heads in the unsaturated zone remain larger than for run 3, which can also be seen in the large maximum head in Fig. 11b.

Our results obtained so far indicate two points: Firstly, we are able to generate a water-table cave, once the water table has dropped to its steady-state position. Secondly, we obtain a flow structure through the unsaturated part of the aquifer, which is controlled by the large aquifer heterogeneities (fractures versus matrix flow), and which can to a certain degree be forced to flow vertically downwards. Still, non-vertical flow components in the unsaturated zone are too large to be realistic. Also, we neglect chemical enlargement in the unsaturated zone, which in reality takes place.
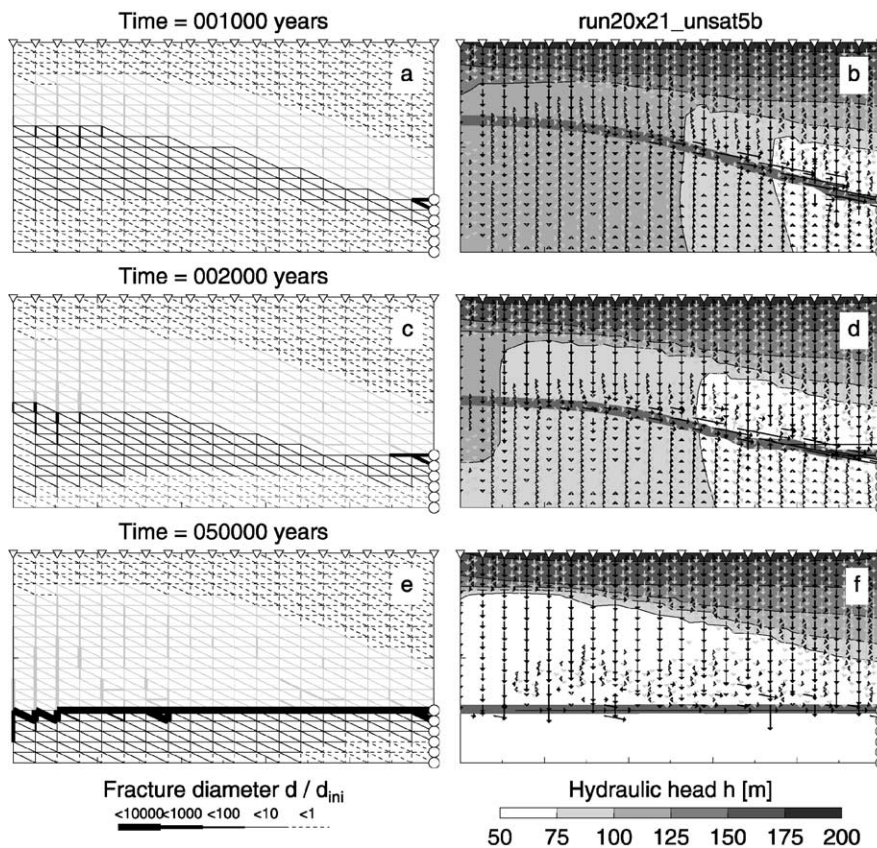

Fig. 10. Run 4: recharge along top boundary (triangles), vadose zone (B, $\alpha = 0.03$), but no dissolution, discharge to base level (dots) along right boundary.
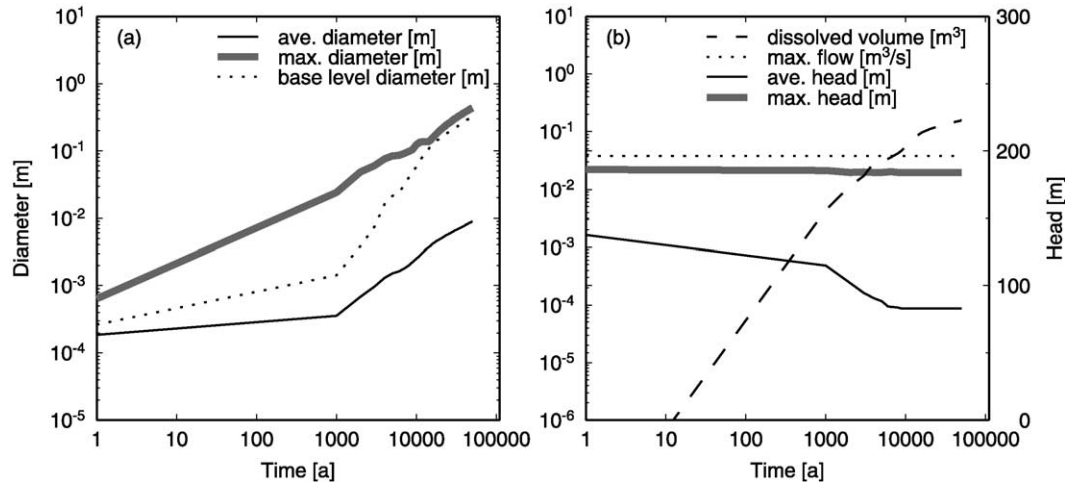
Fig. 11. Run 4: statistical properties.

4.5. Run 5: surface recharge, vadose zone (A, $\alpha = 0.03$) with enlargement

In the fifth run, we apply the conductivity relation introduced with run 3, and additionally allow dissolution in the unsaturated zone, but only for vertical fractures. As no observational data for dissolution rates in the vadose zone are available, we simply assume that the rate law (9) holds both in the phreatic and vadose zones. With this selective enlargement we try to account for the predominantly downward evolution of passages in the vadose zone. Results for this run are shown in Fig. 12a–f. Here we observe from the onset of evolution on the selected enlargement of vertical fractures above the water table, while no horizontal or dipping fractures are enlarged (Fig. 12a). Flow is channelled down effectively through the enlarged vertical fractures (Fig. 12b), and replenishes the water table. Further into the evolution (2000 years, Fig. 12c and d), a zone of enlarged fractures has evolved in the now unsaturated zone, but vertical fractures largely control the flow. At the end of the evolution (50,000 years, Fig. 12e and f), the water table is at its steady-state position and a water-table cave has evolved. Additionally, all vertical fractures in the unsaturated zone are significantly enlarged and channel down the water vertically. Through the vertical enlargement the evolution has bypassed enlarged dipping passages in

the unsaturated zone, which in between have been able to drain the aquifer along the dip-direction (Fig. 12d).

The statistical properties for this run, shown in Fig. 13, reveal the effective vertical enlargement of the unsaturated zone, as both the maximum and the average diameter evolve rapidly in the early phase. In contrast, the evolution of the average diameter of the third run (Fig. 9a) is much slower. The final drop in water table to the steady-state position terminates the early phase and the base-level diameter starts growing and quickly catches up with the maximum diameter. Also, both the average and the maximum heads, while decreasing slowly in the early phase, drop to base-level niveau quickly between 1000 and 10,000 years (Fig. 13b). The large amount of dissolved volume reflects the additional dissolution of the vertical fractures in the unsaturated zone.

4.6. Run 6: surface recharge, vadose zone (A, vertical, $\alpha = 0.2$) with no enlargement

While run 5 already fulfils the two criteria we have imposed, dominant vertical flow within the unsaturated zone and evolution of a water-table cave along the final steady-state water table, the condition to restrict dissolution in the vadose fractures to the vertical dimension is fairly strict. With this sixth run, we provide an alternative
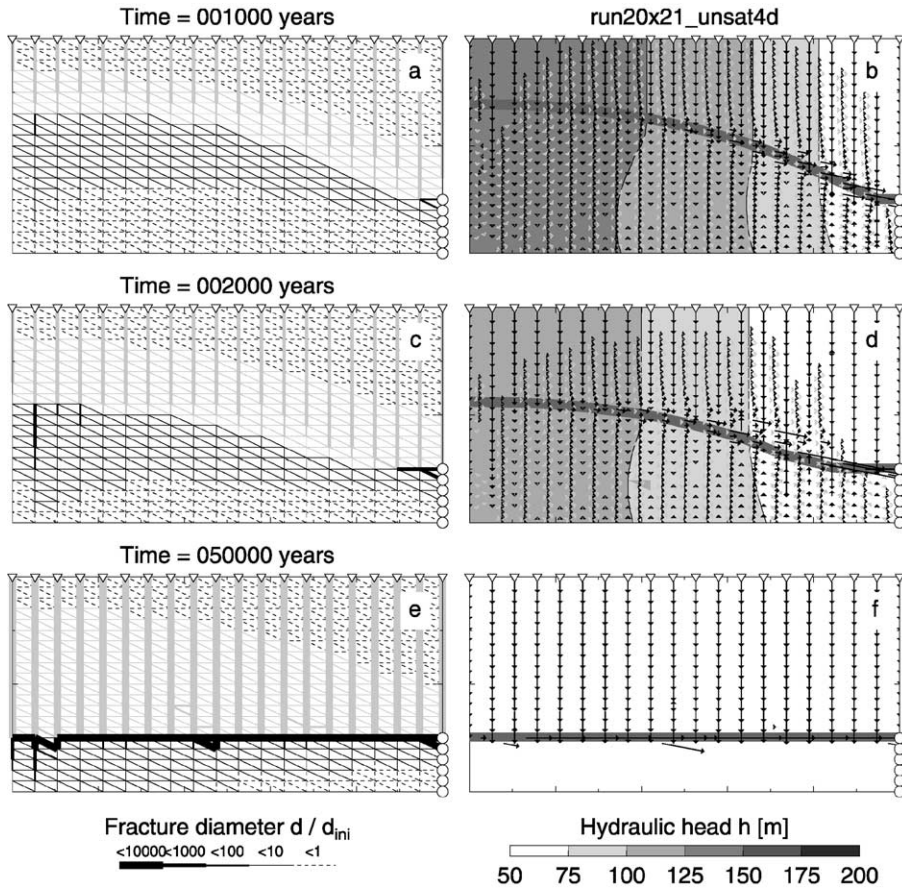
Fig. 12. Run 5: Recharge along top boundary (triangles), vadose zone (A, $\alpha = 0.03$), vertical dissolution, discharge to base level (dots) along right boundary.
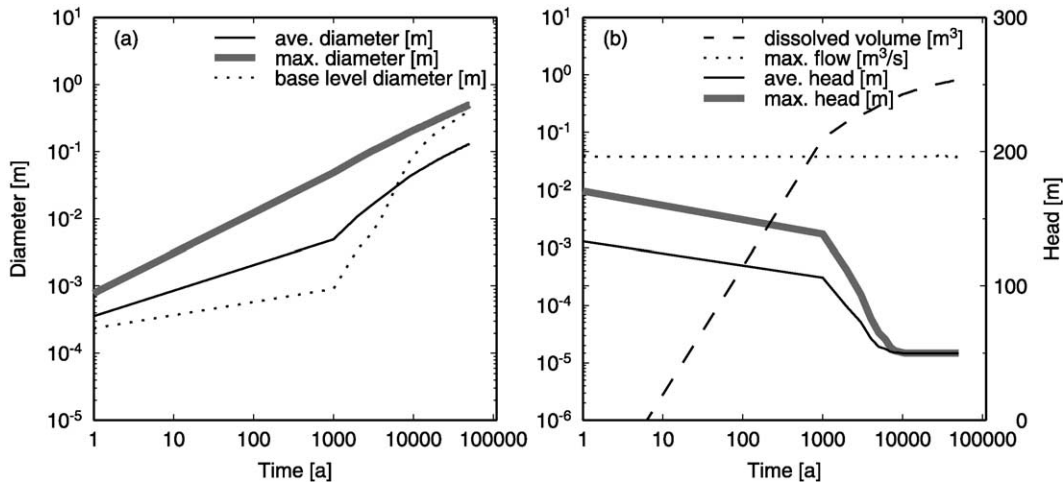

Fig. 13. Run 5: statistical properties.

concept: While dropping the dissolution in the vadose zone again, we now employ relation A in the unsaturated zone only to the non-vertical directions. Hence, flow through the rock matrix becomes non-isotropic, favouring the downward direction. Also, vertical fractures keep their high conductivity, while horizontal and dipping fractures in the vadose zone have a reduced conductivity. Results for this run are shown in Fig. 14a–f. During the early phase (1000 years), fractures have been enlarged under phreatic conditions, but became vadose (Fig. 14a), similar to the previous runs. Differences, however, are visible in the flow field (Fig. 14b): Matrix flow is oriented vertically downward in the unsaturated zone, and along the left side vadose fractures drain vertically down towards the water table. Flow is mainly occurring along the water table. Further into the evolution

(Fig. 14c and d), the water table has dropped significantly, reaching base level along the right side. More importantly, flow through the unsaturated zone is predominantly downward, both in the matrix and the fissure system. Only shortly above the water table flow is redirected along the water table. After 50,000 years (Fig. 14e and f), a prominent water-table cave has evolved, which carries all flow along the stagnant water table towards the resurgence. The unsaturated zone is drained vertically downwards, which matrix flow dominating in the top part (which was never phreatic in the model and hence no fissures are enlarged), and flow through vertical vadose fractures dominating deeper in the unsaturated zone. No deviation from the vertical is present, as all old, now vadose flow pathes marking older water tables are bypassed.
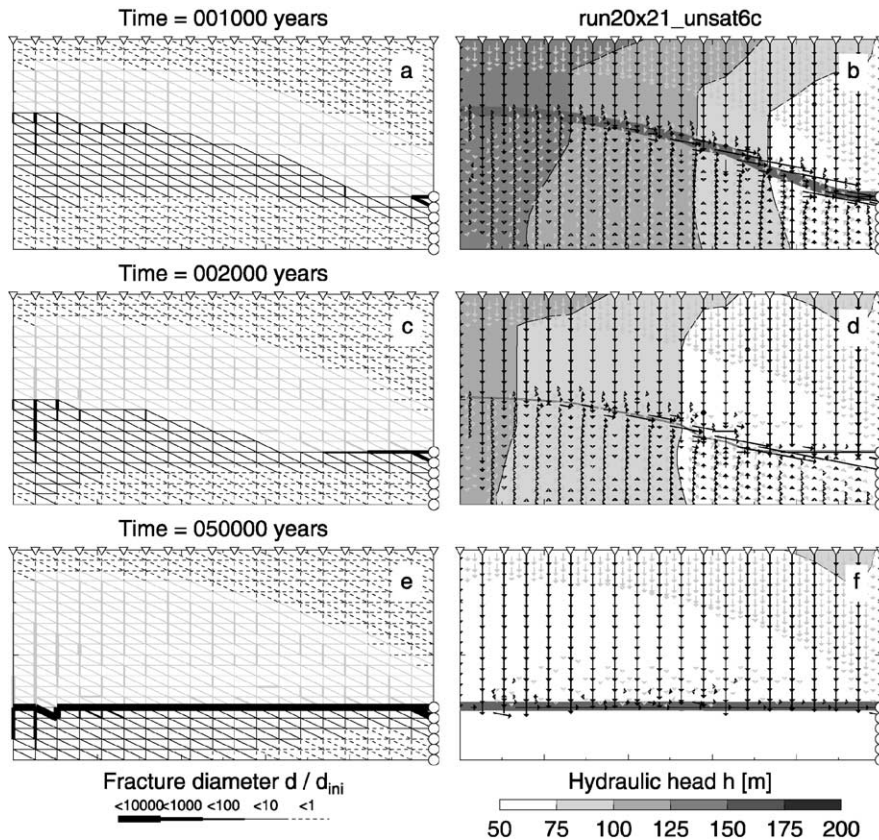

Fig. 14. Run 6: recharge along top boundary (triangles), vadose zone (A, vertical, $\alpha = 0.20$), no dissolution, discharge to base level (dots) along right boundary.
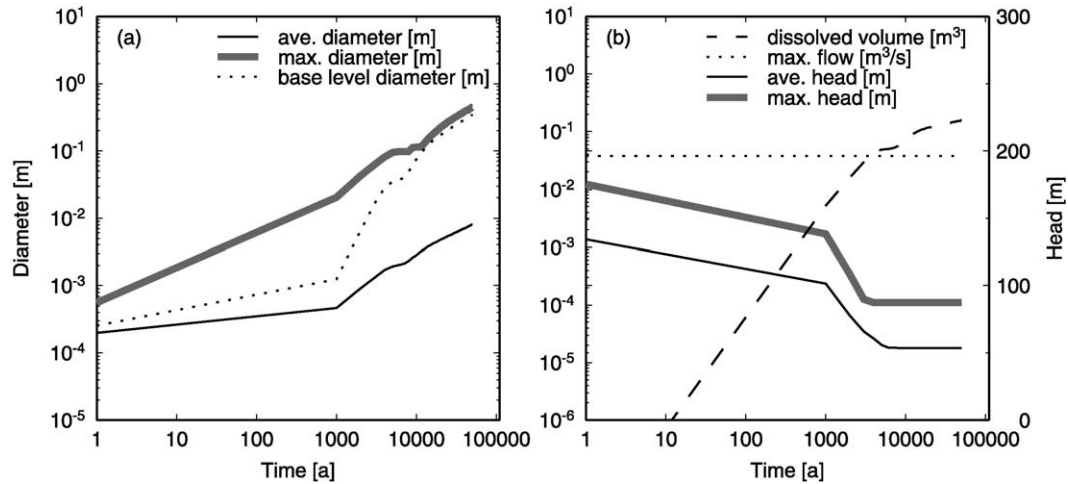
Fig. 15. Run 6: statistical properties.

Statistical properties (Fig. 15) evolve similar as in the first run, the only difference is a slower karstification during the early phase.

5. Discussion and conclusions

The evolution of a karst aquifer in the vertical dimension is controlled by the falling water table. As fractures in the karst aquifer are enlarged with time by chemical dissolution, the aquifer becomes more conductive and the water table drops from an initially high position to a steady-state position on the base-level niveau. Hence, an unsaturated zone is established, as fractures enlarged in the phreatic zone fall dry and become vadose. The enlarged vadose passages, often remnants of an older, higher base-level niveau, are subsequently bypassed by enlarged vertical fractures and shafts, which effectively drain the surface recharge through the vadose zone and replenish the water table.

In this paper, we have included a vadose zone into an evolving vertical karst aquifer model, which is capable of channelling flow down from the surface recharge locations to the water table. Our models, which for the first time include flow through the vadose zone into the aquifer model, can predict the evolution of a water-table cave along the base level, once the water table has dropped to its steady-state position. While the water table is dropping during

the early stages of the evolution, a vadose zone is established, which is characterised by dissolutionally enlarged fractures. As this vadose zone has a highly heterogeneous conductivity, flow through the vadose zone can significantly deviate from the vertical direction. To force the flow vertically downwards through the vadose zone, as it is observed in nature, two approximations can be used: (i) dissolution in the vadose zone is allowed, but in our model needs to be restricted to vertically oriented fractures. This restriction results in the evolution of vertical passages and shafts, which bypass other vadose passages and effectively drain the recharge to the steady-state water table. (ii) The reduction of conductivity in the unsaturated zone is only applied to the non-vertical directions, forcing water vertically downwards through matrix and fractures, also by passing older now vadose passages.

Our model is capable of:

(1) Describing the drop in water table from an initially high to a steady-state position due to the increase in conductivity in the aquifer following the dissolutional enlargement of fractures.
(2) Generating a water-table cave along the final steady-state water table, which grows from the resurgence headwards into the aquifer.
(3) Creating a vadose zone, which is characterised by large-scale heterogeneities in conductivity between enlarged fractures and rock matrix.

(4) Bypassing older vadose cave passages either through the continued vertical enlargement of fractures to shafts, which vertically drain the vadose zone towards the steady-state water table, or through flow forced vertically downwards in the unsaturated zone.

Hence, our model agrees with the water-table cave scenarios presented by Bauer et al. (2000, 2001) and Gabrovsek and Dreybrodt (2001), but it extents these models by explicitly describing both flow in and evolution of the vadose zone. The incorporation of a vadose zone into the numerical models reveals that two processes need to be taken into account during the evolution of the vadose zone: Firstly, the enlargement of fractures, which then subsequently fall dry, establish preferential drainage directions along the enlarged fracture systems, which can redirect water in the enlarged vadose zone from a vertical direction. Secondly, further enlargement in the vadose zone in the vertical direction is needed to bypass the enlarged vadose passages and thus enable the surface recharge to percolate vertically downwards through the vadose zone to replenish the steady-state water table.

Acknowledgements

References

Bauer, S., Liedl, R., Sauter, M., 2000. Threedimensional modelling of karst development considering conduit-matrix exchange flow. Geophys. Res. Abstr. 2, 27.

Bauer, S., Liedl, R., Sauter, M., 2001. Modelling of karst development: effects of recharge distribution. Geophys. Res. Abstr. 3, 2242.

Brooks, R.H., Corey, A.T., 1964. Hydraulic properties of porous media. Technical Report Hydrology paper 3, Civil Engineering Department, Colorado State University, Fort Collins

Clemens, T., Hückinghaus, D., Sauter, M., Liedl, R., Teutsch, G., 1996. A combined continuum and discrete network reactive transport model for the simulation of karst development, Calibration and Reliability in Groundwater Modelling, IAHS Publications, Colorado, Proceedings of the ModelCARE 96 Conference, vol. 237., pp. 309–318.

Clemens, T., Hückinghaus, D., Sauter, M., Liedl, R., Teutsch, G., 1997. Modelling the genesis of karst aquifer systems using a coupled reactive network model, Hard Rock Hydrosciences, IAHS Publications, Colorado, Proceedings of the Rabat Symposium S2, vol. 241., pp. 3–10.

Dreybrodt, W., 1990. The role of dissolution kinetics in the development of karst aquifers in limestone: a model simulation of karst evolution. J. Geol. 98 (5), 639–655.

Dreybrodt, W., 1996. Principles of early development of karst conduits under natural and man-made conditions revealed by mathematical analysis of numerical models. Water Resour. Res. 32 (9), 2923–2935.

Finsterle, S., 2000. Using the continuum approach to model unsaturated flow in fractured rock. Water Resour. Res. 36 (8), 2055–2066.

Gabrovsek, F., Dreybrodt, W., 2001. A comprehensive model of the early evolution of karst aquifers in limestone in the dimensions of length and depth. J. Hydrol. 240 (3–4), 206–224.

Gabrovsek, F., Menne, B., Dreybrodt, W., 2000. A model of early evolution of karst conduits affected by subterranean CO_2 sources. Environ. Geol. 39 (6), 531–543.

Gardner, W.R., Mayhugh, M.S., 1958. Solutions and test of the diffusion equation for the movement of water in soil. Soil Sci. Soc. Am. J. 22, 197–201.

van Genuchten, M.T., 1980. A closed-form equation for predicting the hydraulic conductivity of unsaturated soils. Soil Sci. Soc. Am. J. 44, 892–898.

Groves, C.G., Howard, A.D., 1994a. Minimum hydrochemical conditions allowing limestone cave development. Water Resour. Res. 30 (3), 607–615.

Groves, C.G., Howard, A.D., 1994b. Early development of karst systems 1. Preferential flow path enlargement under laminar flow. Water Resour. Res. 30 (10), 2837–2846.

Gureghian, A.B., 1975. A study by the finite element method of the influence of fractures in confined aquifers. Soc. Pet. Eng. J. 15, 181–191.

Hanna, B.R., Rajaram, H., 1998. Influence of aperture variability on dissolutional growth of fissures in karst formations. Water Resour. Res. 34, 2843–2853.

Howard, A.D., Groves, C.G., 1995. Early development of karst systems 2. Turbulent flow. Water Resour. Res. 31 (1), 19–26.

Huyakorn, P.S., Lester, B.H., Mercer, J.W., 1983. Finite element techniques for modeling groundwater flow in fractured aquifers. Water Resour. Res. 19 (4), 1019–1035.

Istok, J., 1989. Groundwater modeling by the finite element method. AGU Water Resour. Monogr. 13, Washington.

Kaufmann, G., 2002. Karst aquifer evolution in a changing

watertable environment. Water Resour. Res. 38 (6), 261–269.10.1029/2001WR000256.

Kaufmann, G., Braun, J., 1999. Karst aquifer evolution in fractured rocks. Water Resour. Res. 35 (11), 3223–3238.

Kaufmann, G., Braun, J., 2000. Karst aquifer evolution in fractured, porous rocks. Water Resour. Res. 36 (6), 1381–1392.

Mualem, Y., 1976. A new model for predicting the hydraulic conductivity of unsaturated porous media. Water Resour. Res. 12 (3), 513–522.

Palmer, A.N., 1991. Origin and morphology of limestone caves. Geol. Soc. Am. Bull. 103, 1–21.

Siemers, J., Dreybrodt, W., 1998. Early development of karst aquifers on percolation networks of fractures in limestone. Water Resour. Res. 34 (3), 409–419.

Wessel, P., Smith, W.H.F., 1991. Free software helps map and display data. EOS 72, 441–446.

Wessel, P., Smith, W.H.F., 1998. New, improved version of generic mapping tools released. EOS 79, 579.